Supplemental Material for
Acoustic Topological Anderson Insulators

Hui Liu[1], Boyang Xie[1], Haonan Wang[1], Wenwei Liu[1], Zhancheng Li[1], Hua Cheng[1],* Jianguo Tian[1], Zhengyou Liu[2,4],† and Shuqi Chen[1,3‡]

[1]*The Key Laboratory of Weak Light Nonlinear Photonics, Ministry of Education, Renewable Energy Conversion and Storage Center, Smart Sensing Interdisciplinary Science Center, School of Physics and TEDA Institute of Applied Physics, Nankai University, Tianjin 300071, China*

[2]*Key Laboratory of Artificial Micro- and Nanostructures of Ministry of Education and School of Physics and Technology, Wuhan University, Wuhan 430072, China*

[3]*The Collaborative Innovation Center of Extreme Optics, Shanxi University, Taiyuan, Shanxi 030006, China and*

[4]*Institute for Advanced Studies, Wuhan University, Wuhan 430072, China*

(Dated: July 29, 2023)

SUPPLEMENTARY NOTE 1. EFFECT OF THREE PARAMETERS ON TOPOLOGICAL PHASE TRANSITION

We investigated the topological phase transition in a bilayer Lieb lattice model as the function of parameters m, t_0 and t_c. We start with the initial parameters $m = 0.35$, $t_0 = -2$ and $t_c = -0.25$ in a unit cell of bilayer Lieb lattice model corresponding to a trivial phase in the lowest gap. We give the band structure at high-symmetric point M in Fig. S1 (a-c) by varying the parameters m, t_0 and t_c, respectively. The control of m and t_c can support three pairs of degeneracy bands crossing with each other while t_0 does not. Here, we focus on the topological phase transition of the lowest bandgap, where the topology arising from lower two bands are indicated by pink and blue areas for trivial and topological phase, respectively. To confirm the nontrivial topological properties in the model, we calculated the spin Chern number C_s of the lower two bands (green line), middle two bands (red line) and upper two bands (blue line), as plotted in Fig. S1 (d–f). The edge modes at the bandgap originate from the total topological invariants of the lower bulk bands. It is clearly shown that the topological phase transitions occur by control of m and t_c, while it remains unchanged by control of t_0. Although the change of t_0 has no effect on the band structure at high symmetric point M, it can regulate the band structure of other points at the Brillouin zone. The proper regulation of t_0/t_c is conducive to obtain a complete gap. It paves the way for exploring the topological properties of the system when disorder is applied to these parameters.

SUPPLEMENTARY NOTE 2. TOPOLOGICAL ANDERSON PHASE DIAGRAM INDUCED BY DIFFERENT TYPES OF DISORDER

We investigated of the influence of three distinct disorders in a supercell with 21×21unit cell via a bilayer Lieb lattice model. We define $U_{i\in A;\mu} = -(m + \delta U)$, $U_{i\in B,C;\mu} = m + \delta U$, where δU=$[-w/2, w/2]$ and w is disorder strength for m-type disorder. Similarly, $\overline{t_0} = t_0 + \delta t_0$ and $\overline{t_c} = t_c + \delta t_c$ are set for t_0- and t_c- types disorder, respectively. Here, we demonstrate the formation of m- and t_c- types of topological Anderson insulators (TAIs) . We start with a trivial gap by setting the initial parameters $m = 0.35$, $t_0 = -2$, $t_c = -0.25$. Three distinct types of random disorder are added to each unit lattices along both x and y coordinates in the supercell with the hard boundary condition (HBC) and periodic boundary condition

(PBC), respectively. We analyzed the disorder-induced phase diagram described by spin Bott index as the function of different parameters and disorder strength, respectively, as shown in Fig. S2(a,d,g). Although the increasing disorder may result in unreliable results due to indistinguishable gaps, the tendency of topological phase transitions is certain. The spin Bott index in the supercells with PBC changes from 0 to 1 for the m- and t_c- type disorder as the disorder increases, while it remains 0 for the t_0- type disorder. This means that the m- and t_c- types disorder can induce topological phase transitions, while the t_0-type disorder cannot, which are consistent with the TAI mechanism. Setting a specific disorder strength with non-zero spin Bott index denoted by star in Fig. S2(a), we further present the energy eigenvalues in the disorder system with PBC (blue dots) and HBC (red dots), as shown in Fig. S2(b). In the PBC, the total state numbers below the gap are $N_x \times N_y \times 2$, so the gap is the frequency area (cyan) between the state number $N_x \times N_y \times 2$ and $N_x \times N_y \times 2 + 1$. In the HBC, the boundary modes occur in the lowest gap, indicating non-trivial topological phenomenon. The pseudospin dependence of the boundary modes can be determined by their projection into the pseudospin space, represented by color map. The wave function of one boundary mode in the supercell is shown in Fig. S2(c). The energy distribution of eigenstate is localized on the edges of system with HBC, which shows the key hallmark of TAI. The spin Bott index remains zero for the t_0-type disorder with increasing of disorder strength, as plotted in Fig. S2(d). By setting the specific disorder strength indicated by star in Fig. S2(d), the corresponding energy eigenvalues with PBC (blue dots) and HBC (red dots) show a trivial gap denoted by yellow area in Fig. S2(e). in the presence of HBC, several bulk states are disturbed into the gap and one of them has an eigenstate distribution as shown in Fig. S2(f). Finally, we analyze the t_c-type disorder and take the specific disordered strength in the topological phase. We show a topological gap denoted by cyan in Fig. S2(h). The wave function distribution for one of the eigenstates in the gap is plotted in Fig. S2(i), which is localized on the hard boundary of the finite supercell. The appearance of boundary states implies the disorder-driven topological phase transitions. Here, we investigate the mechanism of TAI and answer whether all types of disorder can push a trivial phase to nontrivial, which is not clear in previous works.

SUPPLEMENTARY NOTE 3. THE PSEUDOSPIN SPACE DEFINED IN THE REAL SPACE

To analyze the topological properties in more extensive systems, such as quasicrystals, fractal and disordered systems, we present synthetic spin-orbit coupling and pseudo-spin space defined in the real space. In the disordered supercell with $N_x \times N_y$ unit cells, the bilayer can provide a system with pseudospin of the upper and lower layers. The basis can be taken as $(A_{i,\mu=1}, B_{i,\mu=1}, C_{i,\mu=1}, A_{i,\mu=\text{-}1}, B_{i,\mu=\text{-}1}, C_{i,\mu=\text{-}1})^T$ where $i = 1, \ldots, N_x \times N_y$ denotes the atoms at the ith site on one layer and $\mu \in \{1, \text{-}1\}$ represents the pseudospin of the upper and lower layers. Considering the HBC, we can reduce the Hamiltonian in Eq. (1) into a block matrix form

$$H = \begin{pmatrix} M_A & H_x & H_y & 0 & 0 & 0 \\ H_x^\dagger & M_B & 0 & 0 & 0 & H_+ \\ H_y^\dagger & 0 & M_C & 0 & H_- & 0 \\ 0 & 0 & 0 & M'_A & H_x & H_y \\ 0 & 0 & H_-^\dagger & H_x^\dagger & M'_B & 0 \\ 0 & H_+^\dagger & 0 & H_y^\dagger & 0 & M'_C \end{pmatrix}, \tag{S1}$$

where all the elements are matrices of size $N_x \times N_y$. $M_{A,B,C}(M'_{A,B,C})$ are the diagonal matrices representing the on-site energy of all atoms A, B and C in the upper (lower) layers of the supercell. $H_x(H_y)$ represent the intralayer coupling with strength t_0 between all the atoms A and their nearest-neighbor B or C. $H_+(H_-)$ are the chiral interlayer coupling with strength t_c connecting the nearest-neighbor atoms B or C in the upper layer and the next-nearest-neighbor atoms C or B in the lower layer. We take the unitary transform of the Hamiltonian as $H' = UHU^\dagger$, where $U = \frac{1}{\sqrt{2}} \begin{pmatrix} 1 & -i \\ 1 & i \end{pmatrix} \otimes I_{3\times N_x \times N_y}$, with the unit matrix $I_{3\times N_x \times N_y}$ of size $3 \times N_x \times N_y$. The original Hamiltonian can be transformed into

$$H' = \begin{pmatrix} M_A & H_x & H_y & 0 & 0 & 0 \\ H_x^\dagger & M_B & iH_s & 0 & 0 & -iH_c \\ H_y^\dagger & -iH_s^\dagger & M_C & 0 & -iH_c^\dagger & 0 \\ 0 & 0 & 0 & M'_A & H_x & H_y \\ 0 & 0 & iH_c & H_x^\dagger & M'_B & -iH_s \\ 0 & iH_c^\dagger & 0 & H_y^\dagger & iH_s^\dagger & M'_C \end{pmatrix}, \tag{S2}$$

where $H_s = \left(H_- - H_+^\dagger\right)/2$ and $H_c = \left(H_- + H_+^\dagger\right)/2$. The block matrix H' has a similar form to the Bloch Hamiltonian of spin-Chern crystalline insulator with spin nonconservation [1], in which the bilayer lattice provides a layer pseudospin degree of freedom similar to the intrinsic spin of the electron. H_s term provides a synthetic spin-orbital coupling for the system, which gives rise to the topological nontrivial gap. The topological properties are preserved as long as the pseudospin-mixing term H_c is not strong enough to close the spin-gap. Since the pseudospin operator of H' is naturally $\sigma_z \otimes I_{3\times N_x \times N_y}$, the projected pseudospin operator of the original Hamiltonian H can be determined as $\tau_y = U^\dagger \left(\sigma_z \otimes I_{3\times N_x \times N_y}\right) U = \sigma_y \otimes I_{3\times N_x \times N_y}$. Thus, the concept of spin-orbit coupling and pseudospin space defined in momentum space can be extended to disordered supercell.

SUPPLEMENTARY NOTE 4. THE SPIN BOTT INDEX

Owing to the missing of well-defined bands, the topological properties of the supercell with disorder can be described by the spin Bott index instead of spin Chern number. As the spin Bott index does not depend on any symmetries, it is an effective tool to measure the topological invariants based on real space. The theory of spin Bott index is based on a finite supercell, where the free atoms are located in lattices on a torus, described by a short-ranged, bounded, and gapped Hamiltonian. The calculation of the spin Bott index in a 2D supercell with PBC imposed in two spatial directions [2–6] is described as follows. We analyze the eigenvalue problem for a supercell with the size of $L_x \times L_y = N_x \times N_y \times a^2$, where $a = 1$ is the lattice constant, and $N_{x,y}$ is the number of unit cells. A crucial assumption can be made as: $L_{x,y} \gg a$. The projector operator of the eigenstates below the lowest gap can be expressed as:

$$P = \sum_i^{N_{occ}} |\psi_i\rangle \langle\psi_i|, \tag{S3}$$

where $|\psi_i\rangle$ denotes the eigenstates of the original Hamiltonian H, and N_{occ}=$2 \times N_x \times N_y$ is the number of the occupied states below the gap. The next key step is to separate $N_x \times N_y$ pairs of eigenstates into the pseudospin up and down states. As the projected spin operator of H is τ_y, we project the projector operator (P) into the spin space:

$$P_y = P\tau_y P. \tag{S4}$$

In our systems, the eigenvalues of P_y can be successfully split into two opposite groups ($\pm\hbar/2$) according to pseudospin up and down. The relevant eigenvalue problem can be expressed as:

$$P_y \left|\pm\varphi_i\right\rangle = S_\pm \left|\pm\varphi_i\right\rangle, \tag{S5}$$

where $S_\pm = \pm\hbar/2$. We reconsider the projector operator of the eigenstates with pseudospin up and down, respectively:

$$P_\pm = W_\pm \begin{pmatrix} 0 & 0 \\ 0 & I_{N_x \times N_y} \end{pmatrix} W_\pm^\dagger, \tag{S6}$$

where $W_\pm$ is a unitary matrix comprising the basis vectors $|\pm\varphi_i\rangle$. The corresponding projected position operators in x and y spatial directions for pseudospin up and down are represented as:

$$P_\pm e^{i2\pi X/L_x} P_\pm = W_\pm \begin{pmatrix} 0 & 0 \\ 0 & U_\pm \end{pmatrix} W_\pm^\dagger, \tag{S7}$$

$$P_\pm e^{i2\pi Y/L_y} P_\pm = W_\pm \begin{pmatrix} 0 & 0 \\ 0 & V_\pm \end{pmatrix} W_\pm^\dagger, \tag{S8}$$

where X and Y are diagonal matrices with atomic coordinates in x and y spatial directions as the diagonal elements. One can obtains the matrices $U_\pm = W_\pm^\dagger e^{i2\pi X/L_x} W_\pm$ and $V_\pm = W_\pm^\dagger e^{i2\pi Y/L_y} W_\pm$. The spin Bott indices for pseudospin up and down can be given by:

$$B_\pm = \frac{1}{2\pi} \mathrm{Im}\left\{ Tr\left[\log(V_\pm U_\pm V_\pm^\dagger U_\pm^\dagger) \right] \right\}. \tag{S9}$$

Finally, the spin Bott index can be written as $B_s = \frac{1}{2}(B_+ - B_-)$.

SUPPLEMENTARY NOTE 5. METHODS

All numerical simulations are conducted with a finite element method based on COMSOL MULTIPHYSICS solver package. The systems are filled with air, whose mass density and sound speed at room temperature are 1.18 kg/m^3 and 346 m/s, respectively. Owing to the huge acoustic impedance mismatch compared with air, the 3D printing materials are considered as hard boundaries. The TAI sample is stitched together from three layers of 3D printing structures, including two air layers modulated by square scatterers and a chiral coupling layer connecting them. The detail for the sample fabricated by 3D printing and

experimental set up is shown in Fig. S3. A subwavelength headphone with a diameter of 4 mm is used as sound source in the experiment measurements. The headphone is placed inside the upper layer of sample at the intersection of two hard boundaries for boundary states excitations. A sub-wavelength microphone probe (diameter=3.2mm, B&K Type 4138) was used to measure the acoustic pressure field distributions. A network analyzer (Keysight E5061B 5Hz-500MHz) was used to send and record both the amplitude and phase of the acoustic signals. The dispersions of boundary states were obtained by imposing FFT (Fast Fourier Transformation) to scan acoustic pressure field distributions on the upper layer.

SUPPLEMENTARY NOTE 6. THE FORMATION OF TAI WITH THE INCREASING OF DISORDER

Here, we simulated the topological Anderson phase in TAI sample as the function of disorder strength, which are characterized by the transition of spin Bott index and the occurrence of boundary states. The eigen-frequencies of the acoustic structure with PBC and HBC denoted by blue and red dots are simulated in Fig. S4(a). The topological Anderson phase described by spin Bott index as the function of the disorder strength is shown in Fig. S4(b). Random rotating scatterers introduce both the on-site energy disorder and the in-plane coupling disorder, but only on-site energy disorder induces a topological Anderson phase, and in-plane coupling disorder can ensure an absolute gap. In the PBC, the closure of the gap during the phase transition can be achieved only when the simulated sample size is infinite, which explains why our simulated gap does not close during the phase transition. In addition, the existence of absolute gaps ensures the observation of edge states for sufficiently strong disorder. The topological Anderson phase described by spin Bott index as the function of the disorder strength is shown in Fig. S4(b). With the increasing of disorder strength, the phase in TAI sample is stably located in the topological phase, and the topologically protected boundary states also exist in the gap. The disorder in real acoustic structure varies within a range and cannot indefinitely increase without destroying the lattice as in the tight-binding model, which results in the difference of the topological Anderson phase from that in Fig. S2(a). The major difference is that the disorder in acoustic structure cannot be large enough to bring the topological Anderson phase back to the trivial like the on-site energy disorder in tight-binding model.

In order to demonstrate that topological Anderson phase in TAI sample comes from the on-site energy disorder, we obtain the topological Anderson phase transition consistent with the sample by limiting the on-site energy in tight-binding model to the range of -0.5 and 0.5. The on-site energies beyond this range are set to increase or decrease with the opposite slope. The calculated eigenvalues as a function of disorder strength are given in Fig. S4(c), where the boundary states exist in the gap as the disorder strength increases. The relevant topological phase transition is shown in Fig. S4(d). The system is driven from trivial to nontrivial phase by on-site energy disorder and stays in topological nontrivial phase with the increase of disorder strength, which is consistent with the topological phenomenon in the sample.

SUPPLEMENTARY NOTE 7. PSEUDOSPIN POLARIZATION OF DISORDER-INDUCED BOUNDARY STATES

In order to distinguish the pseudospin polarization of the experimental field distribution of boundary states along x and y directions, we extracted the acoustic field that transmits steadily along both two boundaries and projected them into the pseudospin space, as shown in Fig. S5. The corresponding eigenvalue problem shows that the boundary state propagates along the x and y directions carrying the pseudospin-up and -down polarizations, respectively. The polarization is not strictly close to $+1$ or -1 due to the system without pseudospin conservation and the influence of disorder. Nevertheless, the polarizations can still be split into two opposite groups separated by 0.

* Corresponding author: hcheng@nankai.edu.cn

† Corresponding author: zyliu@whu.edu.cn

‡ Corresponding author: schen@nankai.edu.cn

[1] Weiyin Deng, Xueqin Huang, Jiuyang Lu, Valerio Peri, Feng Li, Sebastian D Huber, and Zhengyou Liu, Acoustic spin-chern insulator induced by synthetic spin–orbit coupling with spin conservation breaking. *Nature communications* **11, 1**, 1–7 (2020).

[2] Terry A Loring and Matthew B Hastings, Disordered topological insulators via c*-algebras. *Europhysics Letters* **92, 6**, 67004 (2011).

[3] Terry A Loring et al., Quantitative k-theory related to spin chern numbers. *SIGMA. Symmetry, Integrability and Geometry: Methods and Applications* **10**, 077 (2014).

[4] Daniele Toniolo, Time-dependent topological systems: A study of the bott index. *Physical Review B* **98, 23**, 235425 (2018).

[5] Huaqing Huang and Feng Liu, Quantum spin hall effect and spin bott index in a quasicrystal lattice. *Physical review letters* **121, 12**, 126401 (2018).

[6] Huaqing Huang and Feng Liu, Theory of spin bott index for quantum spin hall states in nonperiodic systems. *Physical Review B* **98, 12**, 125130 (2018).

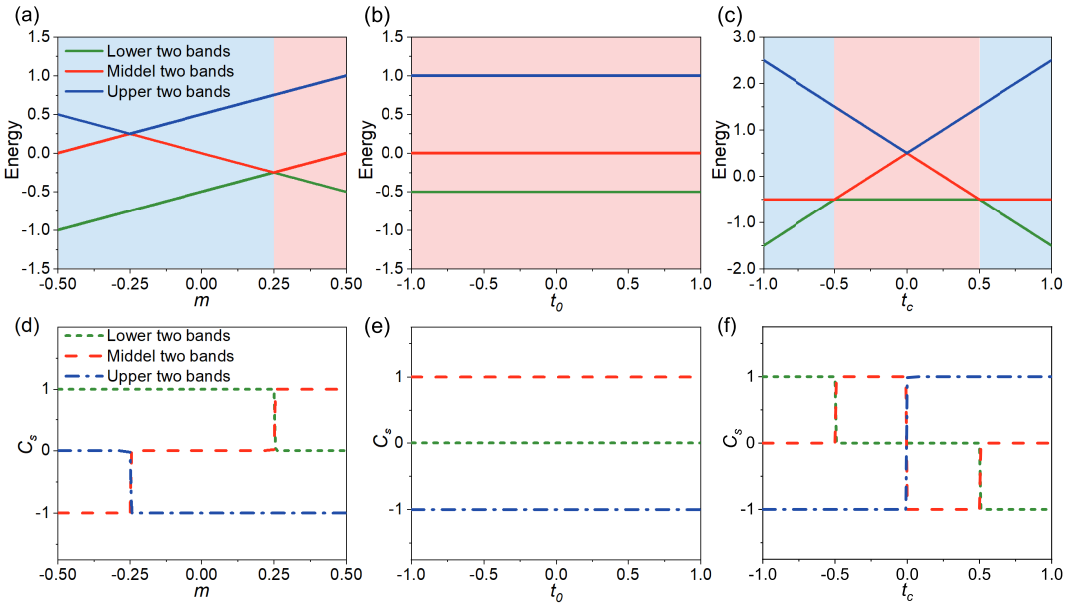

FIG. S1. The bulk bands at high-symmetric point M and the relevant phase transition determined by spin Chern number. The bands at M point as the function of (a) on-site energy m, (b) intralayer coupling t_0 and (c) chiral interlayer coupling t_c. The spin Chern number as the function of (d) on-site energy m, (e) intralayer coupling t_0 and (f) chiral interlayer coupling t_c.

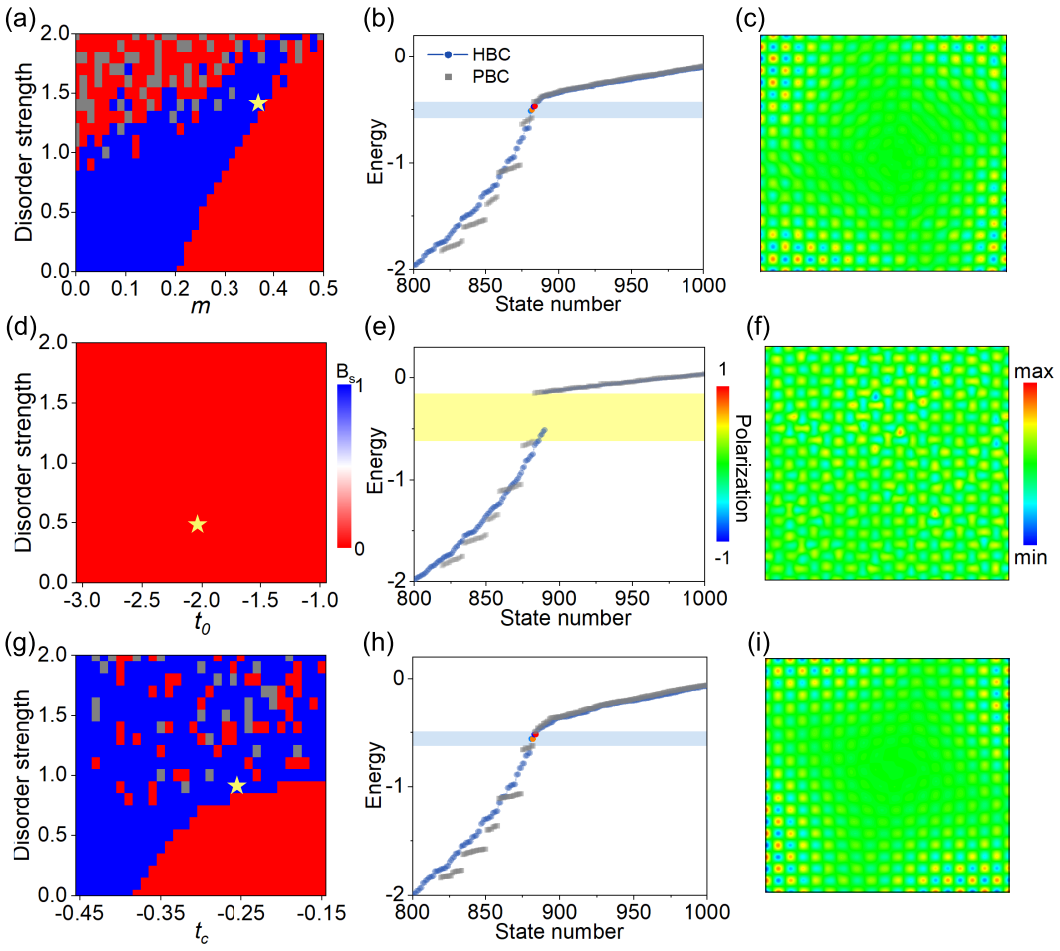

FIG. S2. Phase transitions induced by different type of disorder. Starting with a trivial phase in a supercell model with 21×21 unit cell, the initial parameters are set to $t_0 = -2$, $t_c = -0.25$, $m = 0.35$. (a) Topological Anderson phase diagram for m-type TAI. The yellow star denotes the specific disorder strength used in (b). Gray areas are unreliable results that is removed due to indistinguishable gaps. (b) The supercell with PBC (grey dots) shows a topological gap. In the presence of HBC (blue dots) shows pairs of pseudospin dependent boundary modes in the topological gap denoted by red and blue dots. (c) Field distribution of a typical midgap state in (b), showing the characteristic of boundary mode. (d) Spin Bott index remain zero for t_0-type disorder. (e) Energy eigenvalues with PBC and HBC show trivial gap by setting specific disorder strength represented by red star in (d). (f) Field distribution of a bulk mode with HBC near the gap in (e). (g) Topological Anderson phase diagram for t_c-type TAI. (h) Energy eigenvalues with PBC and HBC show a topological gap, where exist disorder-induced boundary modes with pseudospin up and down polarizations represented by red and blue dots. (i) Field distribution of a typical midgap state in (h), showing a boundary mode.

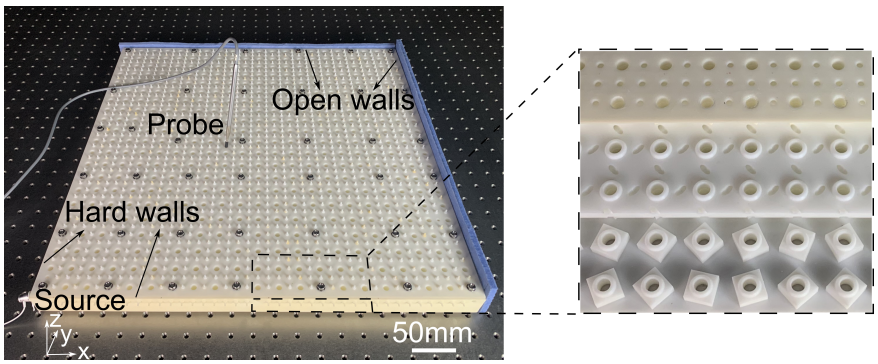

FIG. S3. The experimental set up and sample details. Inset shows the detail of the sample composed of three layers of 3D printing.

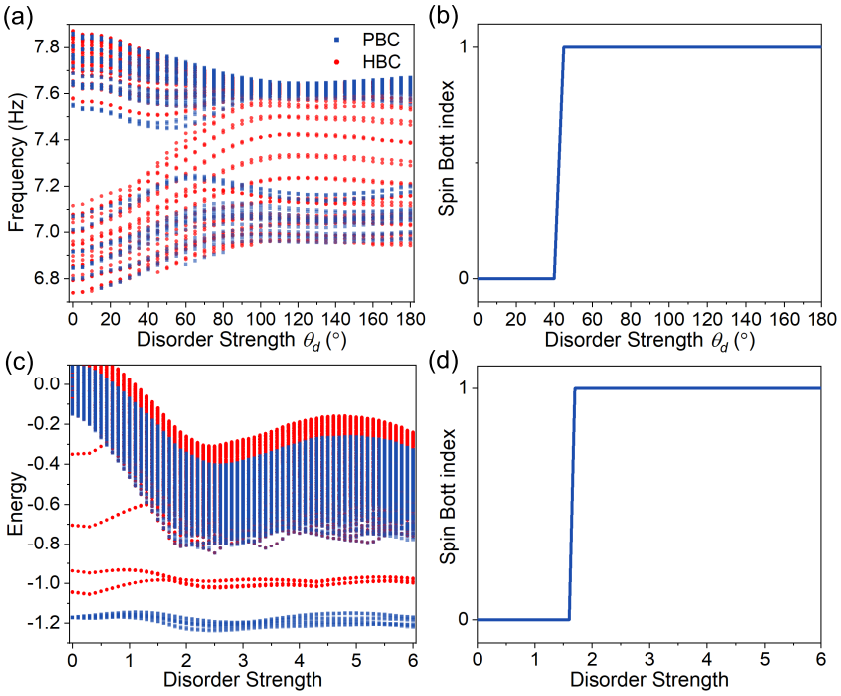

FIG. S4. The formation of TAI with the increasing disorder strength. (a) The simulated eigenvalues for TAI sample as a function of disorder strength, where the blue points and red points represents the eigenvalues with PBC and HBC, respectively. (b) The formation of TAI described by spin Bott index as a function of disorder strength. The red star indicates a specific disorder strength of the sample fabricated in Fig. S3. (c) The eigenvalues for tight-binding model, where on-site energy only varies within a certain range of -0.5 and 0.5. The initial parameters are set to $t_0 = -5$, $t_c = -0.25$, $m = 0.35$. (d) The formation of topological Anderson phase for tight-binding model in (c).

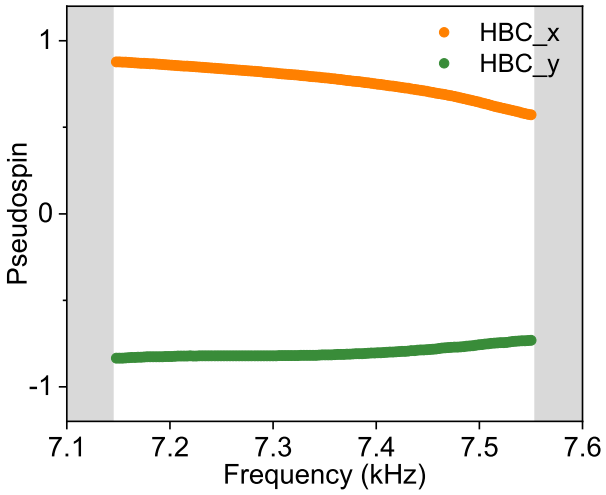

FIG. S5. Pseudospin polarization of excited boundary states. The projection of the x and y direction sound field in the pseudospin space shows positive and negative values respectively, implying that it carries the polarization of pseudospin up (orange) and pseudospin down (green), respectively. The grey areas mean frequencies of bulk modes.